the FEBS Journal

The Ala95-to-Gly substitution in *Aerococcus viridans* L-lactate oxidase revisited – structural consequences at the catalytic site and effect on reactivity with O_2 and other electron acceptors

Thomas Stoisser[1,2], Daniela Rainer[1,2,3], Stefan Leitgeb[1,2], David K. Wilson[3] and Bernd Nidetzky[1,2,4]

1 Research Center Pharmaceutical Engineering, Graz, Austria
2 Institute of Biotechnology and Biochemical Engineering, Graz University of Technology, NAWI Graz, Graz, Austria
3 Department of Molecular and Cellular Biology, University of California, Davis, CA, USA
4 Austrian Centre of Industrial Biotechnology, Graz, Austria

Keywords
electron acceptor; flavin oxygen reactivity; FMN; α-hydroxy acid oxidizing flavoenzymes; L-lactate oxidase

Correspondence
B. Nidetzky, Institute of Biotechnology and Biochemical Engineering, Graz University of Technology, NAWI Graz, Petersgasse 12, A-8010 Graz, Austria
Fax: +43 316 873 8434
Tel: +43 316 873 8400
E-mail: bernd.nidetzky@tugraz.at

(Received 9 October 2014, revised 19 November 2014, accepted 24 November 2014)

doi:10.1111/febs.13162

Aerococcus viridans L-lactate oxidase (avLOX) is a biotechnologically important flavoenzyme that catalyzes the conversion of L-lactate and O_2 into pyruvate and H_2O_2. The enzymatic reaction underlies different biosensor applications of avLOX for blood L-lactate determination. The ability of avLOX to replace O_2 with other electron acceptors such as 2,6-dichlorophenol-indophenol (DCIP) allows the possiblity of analytical and practical applications. The A95G variant of avLOX was previously shown to exhibit lowered reactivity with O_2 compared to wild-type enzyme and therefore was employed in a detailed investigation with respect to the specificity for different electron acceptor substrates. From stopped-flow experiments performed at 20 °C (pH 6.5), we determined that the A95G variant (fully reduced by L-lactate) was approximately three-fold more reactive towards DCIP ($1.0 \pm 0.1 \times 10^6$ $M^{-1}{\cdot}s^{-1}$) than O_2, whereas avLOX wild-type under the same conditions was 14-fold more reactive towards O_2 ($1.8 \pm 0.1 \times 10^6$ $M^{-1}{\cdot}s^{-1}$) than DCIP. Substituted 1,4-benzoquinones were up to five-fold better electron acceptors for reaction with L-lactate-reduced A95G variant than wild-type. A 1.65-Å crystal structure of oxidized A95G variant bound with pyruvate was determined and revealed that the steric volume created by removal of the methyl side chain of Ala95 and a slight additional shift in the main chain at position Gly95 together enable the accomodation of a new active-site water molecule within hydrogen-bond distance to the N5 of the FMN cofactor. The increased steric volume available in the active site allows the A95G variant to exhibit a similar trend with the related glycolate oxidase in electron acceptor substrate specificities, despite the latter containing an alanine at the analogous position.

Database
Atomic coordinates and related experimental data concerning the structure of the A95G variant of *A. viridans* lacate oxidase have been deposited in the Protein Data Bank under the identifier 4RJE.

Abbreviations
avLOX, *Aerococcus viridans* L-lactate oxidase; DCIP, 2,6-dichlorophenol-indophenol; GOX, glycolate oxidase; LOX, L-lacate oxidase; PDB, Protein Data Bank.

Introduction

The α-hydroxy acid-oxidizing enzymes constitute a distinct family of FMN-dependent dehydrogenases and oxidases [1,2]. They share a common $(\beta/\alpha)_8$ TIM barrel fold, with the FMN binding site located at the C-terminal end of the β barrel [3–7]. Enzymes are functional oligomers, typically homotetramers. They catalyze the oxidation of their α-hydroxy acid substrates (e.g. L-lactate, glycolate, L-mandelate) via C-H hydrogen abstraction [8–14], probably via hydride transfer to the oxidized form of FMN [15,16]. The residues involved in FMN binding and forming the active site are highly conserved [3–7], suggesting a common catalytic mechanism of substrate oxidation in the first (reductive) half-reaction of the overall conversion (Fig. 1, Scheme 1). Strikingly, however, individual enzymes differ strongly in how reactive their reduced-state FMN cofactor is towards molecular oxygen. Based on the second-order rate constant for FMN oxidation by O_2 in the second (oxidative) half-reaction, the family is subdivided into a group of highly O_2 reactive oxidases/monooxygenases such as L-lactate oxidase (LOX; 1.8×10^6 $M^{-1}{\cdot}s^{-1}$) [9] and glycolate oxidase (GOX; 8.5×10^4 $M^{-1}{\cdot}s^{-1}$) [8] and another group of dehydrogenases barely reactive with O_2 and including mandelate dehydrogenase [14] and flavocytochrome b_2 [11,12]. Small differences in microenvironment of the reactive C4a-N5 locus of FMN might be responsible [17,18], in part at least, for these starkly varied O_2 reactivities. Enzyme structures [3–7] reveal that strand β1 of the β barrel provides close contact contact with the *re*-face, the side of the flavin ring opposite to where the substrate binds (Fig. 1). A naturally occurring Ala/Gly residue variation within strand β1 is a prominent factor of structural variability around the FMN N5 atom [3–7]. Evidence from site-directed mutagenesis reveals that Ala/Gly residue exchange in different enzymes impacts significantly upon the O_2 reactivity, in addition to having a major effect on the α-hydroxy acid substrate specificity [19–23]. However, the results also show that the Ala/Gly pattern does not constitute a simply addressable oxidase-dehydrogenase switch in α-hydroxy acid-oxidizing flavoenzymes, unlike vanillyl-alcohol oxidases where a similar pattern of Ala and Gly (or Pro) was proposed to determine flavoenzyme activity as a dehydrogenase and oxidase, respectively [24]. Variability in effects caused by the Ala/Gly residue substitution in different α-hydroxy acid-oxidizing enzymes suggests a comparably complex relationship between the catalytic site structure and the control of O_2 reactivity in this flavoenzyme family. To gain a deeper understanding of this relationship, it is essential that the comparative kinetic analysis of wild-type and variant enzymes is complemented by a determination of the corresponding atomic-resolution protein structures.

In the present study, we have focused on the LOX from *Aerococcus viridans* (avLOX), a prototypical oxidase-type member of the α-hydroxy acid-oxidizing flavoenzyme family that has been well characterized biochemically [9,21,25,26] and structurally [6,27–29]. The enzyme is biotechnologically important for its commercialized use in analytical devices for blood L-lactate determination [30,31]. The avLOX catalyzed conversion of L-lactate and O_2 into pyruvate and H_2O_2 provides convenient indirect detection of the analyte via the H_2O_2 that is formed. However, avLOX is also able to replace O_2 by another oxidant such as 2,6-dichlorophenol-indophenol (DCIP), which is exploited in the fabrication and application of L-lactate test strips [32]. An A95G variant of avLOX was previously constructed and shown to exhibit approximately 10-fold lower O_2 reactivity than the wild-type at 4 °C [21]. The mutation was also shown to enhance the enzyme's specificity for long chain and generally larger sized α-hydroxy-acid substrates [21,25].

In competition assays containing DCIP in a concentration matching that of O_2 at air saturation, we noted that the avLOX preference for electron acceptor use in L-lactate oxidation was strongly altered as result of the substitution of Ala95 by Gly: the A95G variant utilized DCIP prior to using O_2, whereas the wild-type enzyme showed reverse-order sequential utilization of

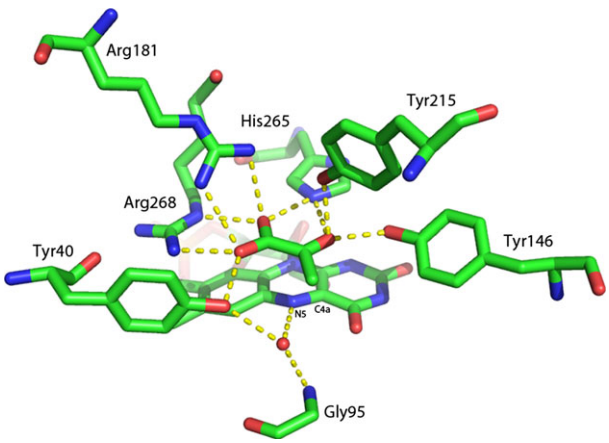

Fig. 1. Close up of the active site of A95G avLOX with bound pyruvate at pH 8.0. The reactive C4a-N5 moiety of the FMN that is involved in hydrogen abstraction from the α-hydroxy acid substrate is indicated. Hydrogen bonds are indicated by dashed lines in yellow. The crystallographic results from the present study are shown. A comparison with the published structure of the wild-type avLOX [27] with Ala95 is considered in the Discussion.

the two electron acceptors present, as expected for a true oxidase. This result therefore suggested 'dehydrogenase-like' behavior of the A95G variant contrary to the wild-type enzyme and prompted further research aiming to clarify the changes in avLOX electron acceptor substrate specificity brought about by the site-directed replacement of Ala95 by Gly. A 1.65-Å crystal structure of A95G variant (FMN oxidized) in complex with pyruvate was determined, and detailed stopped-flow kinetic analysis of the reoxidation of L-lactate-reduced enzymes by different electron acceptors was performed. The A95G variant is shown to place the reactive C4a-N5 moiety of its FMN cofactor into a more hydrated structural microenvironment, somewhat similar to that seen in GOX from the same flavoenzyme family [3], and also, similar to GOX, to exhibit electron acceptor specificities somewhere inbetween an oxidase and dehydrogenase.

Results

A95G avLOX was recombinantly produced in *E. coli* and purified to apparent homogeneity (data not shown). An identical wild-type avLOX is commercially available and, unless stated otherwise, this highly pure recombinant enzyme preparation from *E. coli* was used. However, wild-type avLOX was additionally prepared as described for the A95G variant. To ensure that the preparations of wild-type enzyme obtained commercially and isolated by us were comparable, we performed a relative kinetic characterization of the two. Apparent turnover numbers for L-lactate oxidation at air-saturated oxygen concentration and 37 °C were identical (~ 140 s^{-1}·mol $H_2O_2^{-1}$·mol FMN^{-1}·s^{-1}) and within limits of the experimental error (± 10%). The transient rate constant for oxidation of L-lactate in anaerobic stopped flow experiments at 20 °C (described below) was also identical (220–250 s^{-1}) for the two preparations. Absorbance spectra in the wavelength range 320–600 nm were highly similar for all enzyme preparations, wild-type or A95G variant. However, we noted the relative FMN content of enzyme preparations as isolated was somewhat lower than that of the commercial preparation. Active-site concentrations are therefore always based on the amount of FMN present.

The wild-type avLOX used in the present study differs from the published enzyme structure [6,27] at four sequence positions as a result of substitutions: T102A, S163G, G232A and R255A. None of the substituted residues is close to the active site, nor do they have any reported role in enzyme function or stability.

Change in electron acceptor reactivity as a result of substitution of Ala95 by Gly

When comparing specific enzyme activities determined from initial-rate assays of L-lactate oxidation by DCIP or O_2, we noted the A95G variant to react approximately four-fold faster with DCIP than O_2, in contrast to the wild-type, which showed four-fold higher reactivity with O_2 than DCIP. A faster reaction of A95G variant with DCIP compared to O_2 was also seen when L-lactate was replaced by alternate enzyme substrates such as glycolate (4.2-fold), (*S*)-2-hydroxy-butyrate (5.5-fold) and (*S*)-mandelate (8.2-fold). By comparing O_2 consumption with H_2O_2 formation rates and finding that both rates were identical within limits of experimental error (± 10%), we confirmed that L-lactate oxidation by O_2 followed the uncoupled oxidase path in both wild-type and mutant enzyme (Scheme 1). The alternative coupled path utilized by L-lactate monooxygenase [10,19,20,33,34] where either none or only a small amount of H_2O_2 is released (Scheme 1) was thus ruled out with respect to having any significance under the reaction conditions used. To determine whether the change in relative specific activity caused by the substitution of Ala95 also resulted in altered preference for utilization of DCIP compared to O_2, we performed competition assays in which both electron acceptors were present at a comparable concentration (~ 200 μM) and the time-dependent consumption of each acceptor substrate during L-lactate oxidation was measured. The results shown in Fig. 2 show that DCIP was the preferred electron acceptor substrate for A95G variant, whereas the wild-type clearly preferred O_2.

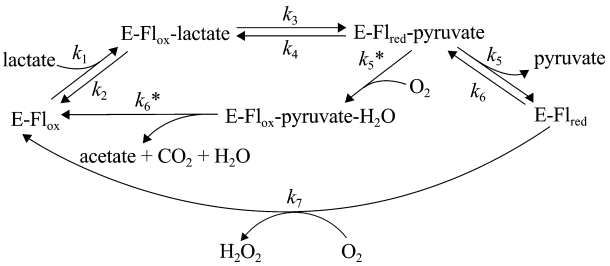

Scheme 1. Proposed reaction pathways of L-lactate oxidase (uncoupled half-reactions: H_2O_2 releasing) and L-lactate monooxygenase (coupled half-reactions: acetate releasing; rate constants marked with asterisk). E-Fl$_{ox}$ and E-Fl$_{red}$ are enzymes with FMN oxidized and reduced, respectively. The scheme is adapted from Maeda-Yorita *et al.* [9].

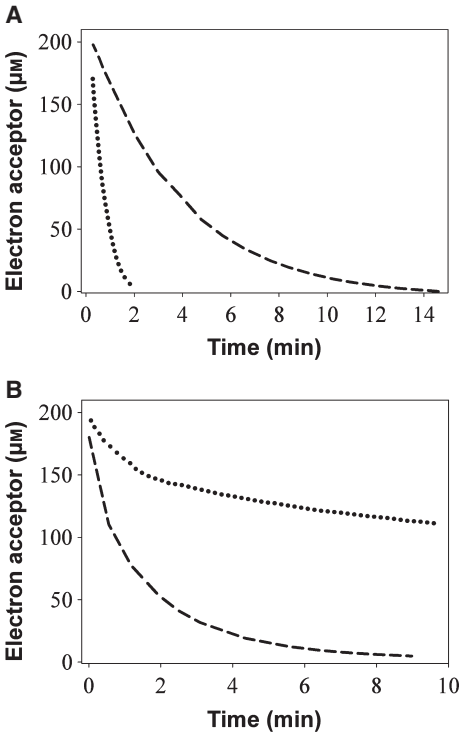

Fig. 2. Utilization of O_2 (dotted line) and DCIP (dashed line) as competing electron acceptors for enzymatic L-lactate oxidation by wild-type (A) and A95G avLOX (B). Reactions were performed at 37 °C using 50 mM L-lactate as substrate. Potassium phosphate buffer (50 mM; pH 6.5) was used. The concentration of wild-type avLOX was 25.6 nM and that of the A95G variant was 7.7 nM. The retardation of O_2 consumption by A95G avLOX at the time when DCIP was largely depleted (≥ 2 min) was noted but not analyzed further.

Kinetics of the reductive half-reaction with different α-hydroxy acid substrates

Anaerobic stopped flow experiments were performed to determine the kinetics of FMN reduction in wild-type and A95G avLOX by L-lactate and also other (bulkier) α-hydroxy acid substrates. Working at 20 °C (Fig. 3), the present study extends earlier mechanistic accounts of the same two enzymes [9,21,25] where the transient kinetic analysis was conducted at 4 °C. With L-mandelate, however, kinetic studies of wild-type and A95G avLOX were subsequently also performed at 25 °C [25].

Irrespective of the substrate and its concentration used, stopped flow absorbance traces at different wavelengths of A95G avLOX were found to be similar to those of the wild-type enzyme, revealing a time-dependent decrease in A_{455} as a result of a progressing reduction of the FMN cofactor (Fig. 3). Unlike at 4 °C, where the formation and decay of reduced enzyme-pyruvate complex (measured at A_{530}) was clearly resolved in time (Fig. 4), stopped flow absorbance traces from reactions at 20 °C did not exhibit similar dynamics of an absorbance band at 530 nm. The proposed pathway of the reductive half-reaction therefore involves Michaelis complex formation, conversion to reduced enzyme–product complex and dissociation of the α-keto acid (Scheme 1). However, the product release step might be too fast at 20 °C to allow for build-up of enzyme–product complex in significant amounts or the elevated temperature prevents detection of such complex. Therefore, under all conditions used at 20 °C, a decrease in A_{455} occurred in a single (exponential) phase (Fig. 3), whereas, in contrast, it was clearly biphasic (bi-exponential) for reactions with L-lactate at 4 °C (Fig. 4). Pseudo-first-order rate constants (k_{obs}) determined from single- or double-exponential fits of stopped flow curves exhibited hyperbolic dependence on the α-hydroxy acid substrate concentration (Fig. 5). Table 1 summarizes the kinetic parameters (k_{red}, K_d) calculated from the data. The results obtained at 4 °C are consistent with Yorita *et al.* [9,21], whereas differences in parameter values are attributed to varied buffer and pH conditions as used in the present study and in the earlier study. Buffer effects have been noted in earlier studies of different α-hydroxy acid oxidases [10,35]. The k_{red} for oxidation of L-lactate was similar for wild-type and A95G avLOX. Binding of L-lactate (K_d) was weakened 7.4-fold as result of the mutation. In k_{red} terms, the A95G variant was much more reactive than wild-type enzyme when used with the substrates (*S*)-mandelic acid (66-fold) and (*S*)-2-hydroxy butyric acid (41-fold). The improved reactivity of these bulky α-hydroxy acid substrates was mainly the result of an increase in k_{red}.

Kinetics of the oxidative half-reaction using different electron acceptors

Reoxidation of the reduced lactate oxidases was measured in stopped flow experiments at 20 °C using different electron acceptors applied under varied concentrations. Stopped flow absorbance traces recorded at different wavelengths indicated the complete reoxidation of both enzymes under all conditions used. Figure 3 shows the oxidation of wild-type avLOX by DCIP as an example. An increase in A_{455} occurred in a single (exponential) phase from which k_{obs} was determined. The k_{obs} was also determined from the corresponding decrease in DCIP A_{600} (Fig. 3) and the k_{obs} values obtained from measurements of A_{455} and A_{600} agreed within the limits of error (typically ±10%). Unless explicitly noted, however, the k_{obs} data are from stopped flow absorbance traces at A_{455}.

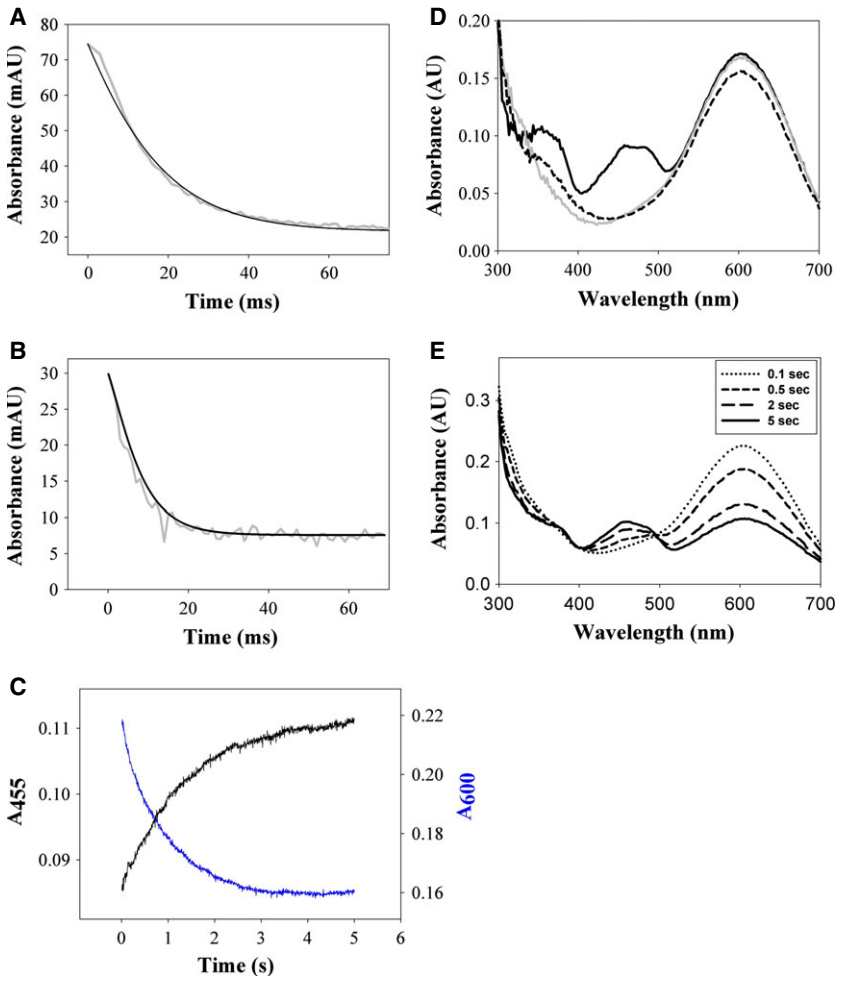

Fig. 3. Kinetic analysis of reduction and re-oxidation of FMN in avLOX analyzed in anaerobic stopped flow experiments at 20 °C. (A, B) Single wavelength traces of FMN reduction (455 nm) in wild-type (A, 6 μM; 2 mM L-lactate) and A95G avLOX (B, 3 μM; 12.5 mM L-lactate). The grey traces show the measurements and the black lines are single exponential fits to the data. (C) Single wavelength traces of FMN re-oxidation (455 nm; black) by 25 μM DCIP (600 nm; blue) using L-lactate reduced enzyme (5 μM). Single exponential fits of averaged traces for the increase in A_{455} and decrease in A_{600} gave values of k_{obs} that agreed within 10%. (D) Enzyme (5 μM) absorbance spectra recorded in 50 mM potassium phosphate buffer (pH 6.5) in the presence of 25 μM DCIP, for oxidized enzyme (black line), enzyme reduced by the molar equivalent of L-lactate (black dashed line) and dithionite-reduced enzyme (grey line). (E) Superimposition of time-resolved absorbance spectra recorded during the reoxidation of L-lactate-reduced enzyme (6 μM) by 30 μM DCIP.

The k_{obs} values exhibited a linear dependence on the acceptor substrate concentration used (Fig. 6). The second-order rate constant k_{ox} was obtained as the slope of straight-line fit to the data (Fig. 6). A summary of the kinetic parameters is provided in Table 2.

The O_2 reactivity was decreased 5.5-fold in A95G compared to wild-type avLOX, confirming evidence obtained in the study reported by Yorita *et al.* [21] as performed at 4 °C. The reactivities of alternative electron acceptors, however, were higher with A95G than wild-type avLOX: DCIP (7.7-fold); 2,5-dichloro-1,4-benzoquinone (3.3-fold); and 2-methyl-1,4-benzoquinone (4.3-fold). The electron acceptors used spanned a representative range of standard redox potentials from +0.176 V to +0.281 V (Table 2). Unlike other flavoenzymes in which the k_{ox} exhibited clear dependence on acceptor substrate redox potential [38], the k_{ox} values of the reduced lactate oxidases did not reveal a recognizable trend correlation that would have supported quantitative structure–activity relationship analysis.

Crystal structure of A95G avLOX

The A95G avLOX crystal structure was determined and the crystallographic data collection and refinement statistics are summarized in Table 3. As with the wild-type structure [6,27], the A95G avLOX structure is tetrameric with an entire C_4 tetramer within the asymmetric unit. Disorder prevented the fitting of residue ranges in each subunit in the final refined model: A (1–5, 203–204), B (1–6, 199–204), C (1–7, 203–204, 214–217), D (1–7, 203–204). FMN cofactors and pyruvates were found in locations consistent with the wild-type structure [Protein Data Bank (PDB) accession number: 2E77] [27]. Unless stated otherwise, structural analysis was carried out using subunit A (Fig. 7) because the overall B-factors for each subunit (A: 13.6 Å^2; B: 14.9 Å^2; C: 14.5 Å^2; D: 14.0 Å^2) indicated that it had the lowest disorder. These subunits are similar overall with the r.m.s.d. of C_αs from subunit A calculated to be 0.26, 0.21 and 0.16 Å, respectively, for subunits B, C and D. As previously determined, the

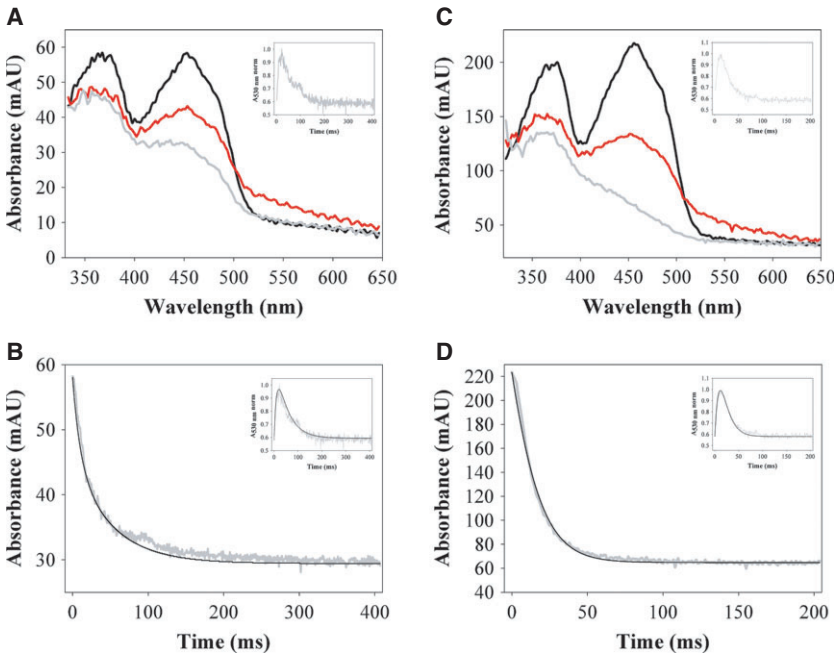

Fig. 4. Reductive half-reaction of A95G avLOX analyzed in enzyme-monitored turnover experiments at 4 °C in 50 mM potassium phosphate buffer (pH 6.5). (A) Enzyme (5 μM) absorbance spectra at reaction start (black line) and after mixing with 8 mM L-lactate and reaction for 18 ms (red line). The grey line shows the spectrum after reaction for 200 ms. Inset shows the time-resolved absorption trace at 530 nm, normalized on the maximum absorption observed at this wavelength in the reaction. According to previous studies of avLOX [9,21], the change in the 530-nm band is a result of the formation and decay of a complex between reduced enzyme and pyruvate, and the inset shows the dynamics of the complex. (B) Stopped flow trace at 455 nm monitoring FMN reduction, with the inset showing the corresponding trace at 530 nm. Solid lines are fits of Scheme 1 for anaerobic L-lactate oxidation (steps k_1 to k_6) to the data using the differential equation solver BERKELEY MADONNA, version 8.3.18 (www.berkeleymadonna.com). (C, D) The same analysis carried out for wild-type avLOX with the exception that 10 mM L-lactate and 19.4 μM enzyme were used. In (C), the red line shows the reaction after 14 ms. Useful fits were obtained with the rate constants: A95G variant: k_2/k_1 = 6 mM, k_3 = 77 s^{-1}, k_4 = 0 s^{-1}, k_5 = 24 s^{-1} and k_6 = 10 $mM^{-1}{\cdot}s^{-1}$. Wild-type: k_2/k_1 = 1 mM, k_3 = 88 s^{-1}, k_4 = 0 s^{-1}, k_5 = 87 s^{-1} and k_6 = 10 $mM^{-1}{\cdot}s^{-1}$. Rate constants k_3 and k_5 agree reasonably with the k_{obs} data obtained from double-exponential fits of the absorbance trace at 455 nm (Table 1).

overall fold is a $(\beta/\alpha)_8$ barrel and the active site is found adjacent to the FMN cofactor at the C-terminal end of the inner β barrel (Fig. 7). In addition to the A95G substitution, this protein contains four other residue replacements (T102A, S163G, G232A and R255A), which distinguish it from the reported avLOX structure [27]. In most cases, these were well defined in the electron density. From a structural perspective, they are likely to be functionally inert because they are all on the periphery of the structure and > 18 Å from the oxidized substrate carbon on the pyruvate in the active site (Fig. 7). The pyruvate occupying the active site is almost completely sequestered from solvent by the loops connecting strands and helices, as well as by two longer irregular excursions composed of amino acids 34–44 and 179–218. One or more of these loops must therefore move to allow substrate binding and product exit. We note B-factors trend higher for amino acids in this second loop, particularly in subunits B and C, suggesting that the mobility of some or all of these residues is important with respect to access to the active site of the enzyme.

A comparison of the structure of the pyruvate-bound A95G and wild-type active sites reveals almost identical structures (Figs 1 and 8A). In particular, there are no changes in any of the residues within van der Waals contact of the pyruvate (i.e. Tyr40, Tyr124, Tyr146, Arg181, Tyr215, His265 or Arg268). There is a significant change in the main-chain conformational torsion angles of Gly95 relative to the wild-type enzyme, leading to a 0.8-Å displacement of the α-carbon, creating somewhat more volume adjacent to the pyruvate methyl binding site. The missing methyl group in the wild-type alanine is replaced with a water molecule that hydrogen bonds with N5 of the isoalloxazine ring (Figs 1 and 8A).

The FMN cofactor is bound at the C-terminal end of the internal β-barrel and interactions between it and the enzyme are almost identical to those found in the wild-type structure. One notable difference is the

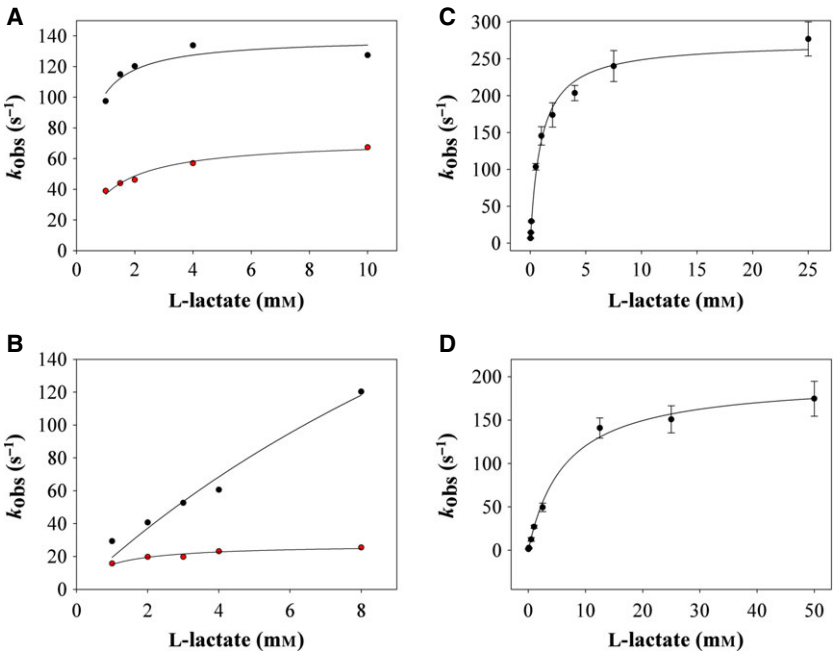

Fig. 5. Dependencies of pseudo-first-order rate constants of anaerobic enzyme-monitored turnover at 4 °C (A, B) and 20 °C (C, D) on the L-lactate concentration. (A, C) Results of reductive half-reactions of wild-type avLOX. (B, D) Results of reductive half-reactions of A95G variant. The shown k_{obs} values are from fits of double- (A, B) and single- (C, D) exponential decay functions to stopped-flow absorbance traces (455 nm) of FMN reduction. Black and red symbols show k_{obs} values associated with the fast and slow kinetic transient, respectively. Solid lines show hyperbolic fits of the data, giving rise to a k_{red} value at saturating L-lactate and a dissociation constant of L-lactate (K_d). Values of k_{red} and K_d for the fast and slow reduction phase are summarized in Table 1.

Table 1. Kinetic constants of FMN reduction by α-hydroxy acid substrate in wild-type and A95G avLOX determined in enzyme-monitored anaerobic stopped flow experiments using 50 mM potassium phosphate buffer (pH 6.5) at 20 °C. ND, not determined.

	Enzyme	
Substrate	Wild-type	A95G
L-Lactate		
At 20 °C		
k_{red} (s^{-1})[a]	274 ± 11	235 ± 13
K_d (mM)[b]	1.0 ± 0.2	7.4 ± 1.5
At 4 °C		
k_{red1} (s^{-1})[c,d]	138 ± 6	142 ± 16
k_{red2} (s^{-1})[c,d]	72 ± 3	27 ± 1
K_{d1} (mM)	0.35 ± 0.10	5.0 ± 1.0
K_{d2} (mM)	1.0 ± 0.1	0.8 ± 0.2
(*S*)-Mandelic acid		
k_{red} (s^{-1})	0.08 ± 0.01	5.3 ± 0.5
K_d (mM)	ND	0.6 ± 0.2
(*S*)-2-Hydroxybutyric acid		
k_{red} (s^{-1})	9.0 ± 0.5	398 ± 28
K_d (mM)	0.9 ± 0.2	2.3 ± 0.4

[a] From Scheme 1, the measured k_{red} is an expression of k_3 and k_5. Equality of k_3 and k_5 is inferred from the fact that FMN reduction occurred in a single exponential phase. Therefore, the value for k_3 and k_5 is 274 s^{-1} (= k_{red}).

[b] From Scheme 1, K_d is the substrate dissociation constant defined as the ratio of k_2/k_1.

[c] From Scheme 1, k_{red1} is k_3 and k_{red2} is k_5.

[d] Fits of increase and decrease of A_{530} for the reaction at saturating L-lactate concentration (20 mM) gave similar (±15%) values of k_{red1} and k_{red2}, respectively.

planarity of the flavin ring. The prior structure appears to be refined as a planar ring system with C7 and C8, two peripheral methyl groups allowed to diverge slightly from the plane. Attempts to refine the A95G structure with strict planarity restraints being imposed resulted in clear residual electron density, which was consistent in all four monomers, showing that the rings were not planar in this case. The final structure resulted in a flavin ring with an approximately 18° 'butterfly angle', which is within the range of 0–34° found in other examples of reduced flavin ring systems [39]. This FMN structure is clearly more consistent with the unbiased high-resolution electron density (Fig. 9). Crystals were grown and maintained in an ambient air environment, which should strongly promote the oxidized form of the cofactor; however, photoreduction of flavins during X-ray exposure appears to be a widespread phenomenom and provides a likely explanation for the lack of FMN planarity seen in all four subunits of the A95G structure [40]. The possibility therefore exists that the FMNs are present in a one-electron-reduced form. However, the collection of further evidence supporting the tentative semiquinone state of the FMN in the structure was beyond the scope of the present study.

Discussion

Determination of the mechanistic implications of Ala/Gly residue variation at the active site of

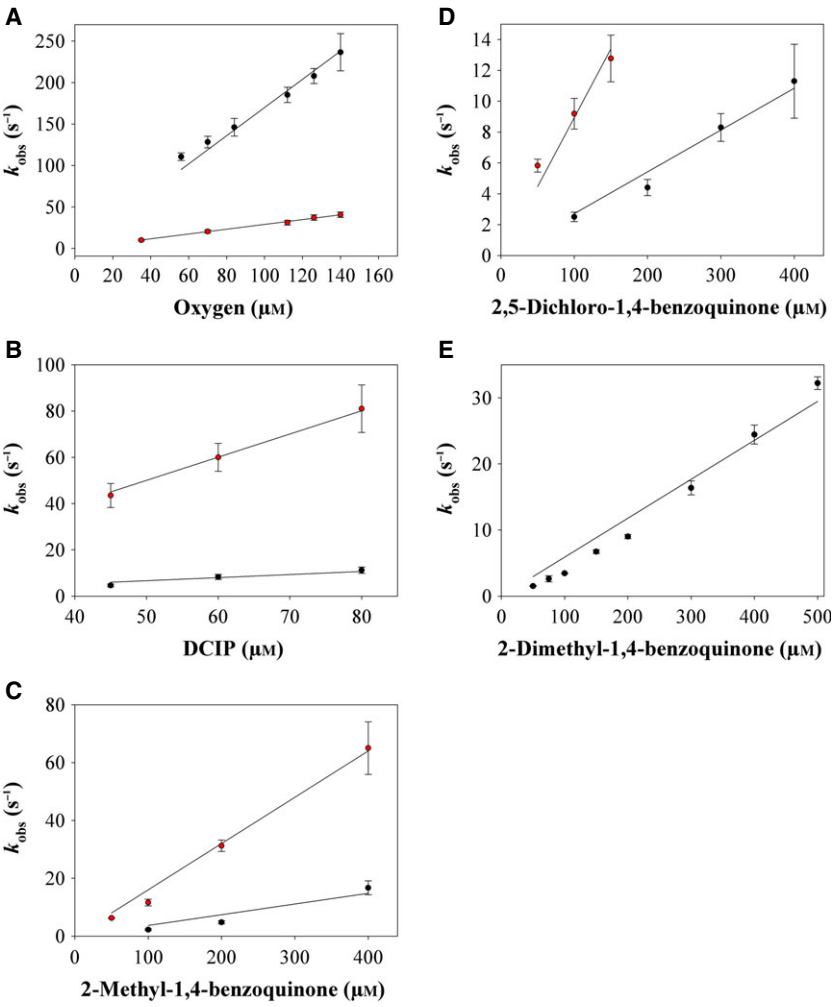

Fig. 6. Kinetic analysis of re-oxidation of reduced FMN in avLOX wild-type and A95G by different electron acceptors (A-E) in 50 mM potassium phosphate buffer (pH 6.5) at 20 °C. Enzyme (10 μM) was reduced anaerobically by L-lactate (20 μM) and then mixed with electron acceptor at the final concentration indicated. Absorbance traces at 455 nm were fitted with single exponentials to obtain k_{obs}. Red circles show A95G; black circles show wild-type avLOX. Error bars indicate the SD from three independent experiments. Straight-line fits of the data are shown and used to obtain k_{ox} (Table 2).

α-hydroxy acid-oxidizing flavoenzymes promises a deeper insight into the role of the microenvironment of the FMN cofactor's reactive C4a-N5 locus on the efficiency of each catalytic step of the enzymatic reaction. Reactivity in the oxidative half-reaction with O_2 compared to reactivity with alternative electron acceptors distinguishes oxidase from dehydrogenase-type members of the family and is therefore considered particularly relevant. Identification of the structural principles of O_2 reactivity is of high current interest in mechanistic flavoenzyme research in general [17,18,41,42].

The replacement of Ala95 by Gly in avLOX has already been described in the literature and its functional consequences have been analyzed in considerable detail [21,25]. These prior studies notwithstanding, the present study represents a significant advance via A95G avLOX structure determination, which, for the first time, enables an interpretation of the kinetic consequences of the site-directed substitution, as obtained in the present study and in previous studies [21,25], in terms of changes in active-site conformation induced. Detailed kinetic analysis of the reoxidation of wild-type and A95G avLOX revealed previously unknown effects of the mutation on modulating enzyme specificity for the reaction with different electron acceptor substrates. These findings are relevant in connection to the oxidase/dehydrogenase dichotomy in α-hydroxy acid-oxidizing flavoenzymes. Structures of relevant Ala-to-Gly (flavocytochrome b_2) [43] and Gly-to-Ala (mandelate dehydrogenase) [44] mutants of dehydrogenase-type members of the enzyme family are available, although the structural consequences of the same mutation in an oxidase from this family have not been reported.

Reaction pathway of L-lactate oxidation by O_2

Kinetic data for L-lactate oxidation by wild-type and A95G avLOX at low (4 °C) and ambient (20 °C)

Table 2. Kinetic constants of FMN reoxidation by different electron acceptors in wild-type and A95G avLOX determined at 20 °C in enzyme-monitored stopped flow experiments using 50 mM potassium phosphate buffer (pH 6.5). Enzyme (10 μM) was reduced by L-lactate (20 μM) in the first reaction step performed anaerobically. ND, not determined.

Electron acceptor	E_m[a] (V)	Wild-type k_{ox} ($M^{-1}\cdot s^{-1}$)[d,e]	A95G
2,5-Dichloro-1,4-benzoquinone	+0.310	$2.7 \pm 0.2 \times 10^4$	$8.9 \pm 0.5 \times 10^4$
2-Methyl-1,4-benzoquinone	+0.251	$3.7 \pm 0.2 \times 10^4$	$1.6 \pm 0.1 \times 10^5$
2,6-Dichlorophenolindophenol	+0.217[b]	$1.3 \pm 0.1 \times 10^5$	$1.0 \pm 0.1 \times 10^6$
2,5-Dimethyl-1,4-benzoquinone	+0.176	$5.9 \pm 0.4 \times 10^4$	ND
O_2/H_2O_2	+0.281[c]	$1.8 \pm 0.1 \times 10^6$	$3.3 \pm 0.2 \times 10^5$

[a] E_m is the midpoint reduction potential (30 °C, pH 7.0) from Rao and Hayon [36].
[b] E_m is the midpoint reduction potential (30 °C, pH 7.0) from Dawson *et al.* [37].
[c] E_m is the midpoint reduction potential (30 °C, pH 7.0) from Mattevi [17].
[d] k_{ox} is the second-order rate constant of FMN re-oxidation determined from linear dependencies of pseudo-first-order stopped flow rate constants, as shown in Fig. 3. Standard errors are from straight-line fits of the data.
[e] From Scheme 1, k_{ox} equals k_7.

Table 3. Crystallographic data collection and refinement statistics. Values given in parentheses are for data in the high-resolution bin.

Data collection	
Unit cell dimensions	
a, *b*, *c* (Å)	122.59, 124.36, 106.89
β (°)	124.29
Resolution range (Å)	50.00–1.65 (1.68–1.65)
Completeness (%)	98.2 (95.1)
R_{merge}	5.9 % (37.1 %)
Observations/unique reflections	581 586/155 981
Mean I/σ (I)	26.4 (4.1)
Refinement statistics	
R_{work} (%)	15.2
R_{free} (%)	18.0
R_{free} test set	7791
Deviations from ideal geometry	
Bond lengths (Å)	0.013
Bond angles (°)	1.54
Average B values (Å^2)	
Main-chain atoms	13.1
Side-chain atoms	15.3
FMN	10.3
Water molecules (920)	19.3
All atoms	14.6
Ramachandran plot (%)	
Most favoured	96.6
Additionally allowed	3.0
Outliers	0.4

temperature suggest a common reaction pathway for both enzymes, as shown in Scheme 1. Evidence suggesting that reduced lactate oxidases were not detectably oxidized by excess of pyruvate under anaerobic conditions at 20 °C indicated that, practically, $k_4 \sim 0$. Model fits to anaerobic stopped flow curves at 4 °C (Fig. 4) also suggested that the reverse reaction from pyruvate was not significant under the conditions used, which is consistent with the literature [21,25]. (Note that microscopic reversibility of α-hydroxy acid/α-keto acid interconversion is not called into question and was clearly shown for reactions catalyzed by mandelate dehydrogenase [45] and flavocytochrome b_5 [46]. However, oxidation of flavocytochrome b_5 by pyruvate occurred with a rate constant of only 0.08 s^{-1}). Therefore, the apparent turnover number of the lactate oxidases at air-saturated reaction conditions (k_{cat_app}) is described with rate constants from Scheme 1 [19,20]:

$$k_{cat\_app} = 1/[(k_3 + k_5)/(k_3k_5) + 1/(k_7[O_2])] \quad (1)$$

Using a value of 250 μM for $[O_2]$ and applying the relevant rate constants from Tables 1 and 2, the calculated k_{cat_app} of wild-type avLOX is 105 s^{-1}, which is in useful agreement with the k_{cat_app} value of 88 s^{-1} obtained from steady-state kinetic analysis conducted at the same $[O_2]$. For the A95G enzyme, the calculated k_{cat_app} of 48 s^{-1} was somewhat higher than the experimental value of 30 s^{-1}.

The K_m for oxygen and L-lactate can also be calculated:

$$K_m(O_2) = k_3k_5/[k_7/(k_3 + k_5)] \quad (2)$$

$$K_m(\text{L-lactate}) = [(1/k_1) + k_2k_5/(k_1k_3k_5)]/(1/k_{cat\_app}) \quad (3)$$

Values of 69 and 356 μM are thus obtained for K_m (O_2) of wild-type and A95G avLOX, respectively. The calculated K_m (L-lactate) values are 0.71 and 1.5 mM

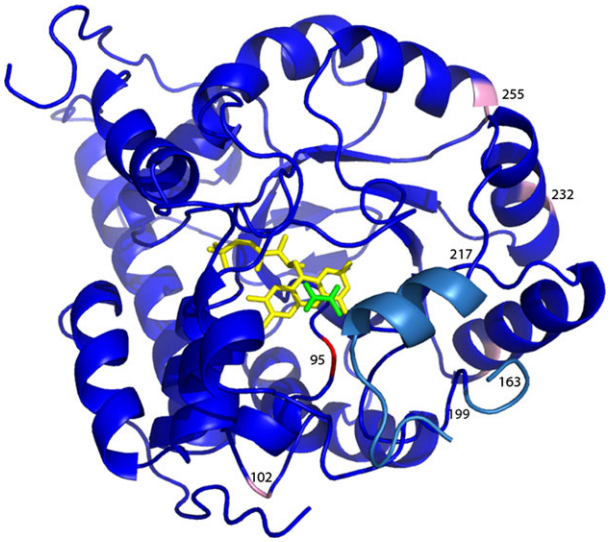

Fig. 7. The Cα trace of the A subunit of A95G avLOX (blue) showing the position of the FMN (yellow), the pyruvate (green), the sites of the inert mutations (T102A, S163G, G232A and R255A, pink) and the active site A95G mutation (red). The stretch of residues from 199–217 with a higher mobility in some subunits is indicated in light blue.

for wild-type and A95G avLOX, respectively, and can be compared to the corresponding values of 0.5 ± 0.1 mM and 1.0 ± 0.2 mM obtained from steady-state kinetic analysis.

Comparison of active-site structures and electron acceptor reactivities of A95G avLOX and glycolate oxidase

Similar to A95G avLOX, GOX is also able to efficiently utilize electron acceptors different from and larger than molecular oxygen. For example, GOX from pig liver was reported to exhibit a two-fold higher turnover number with DCIP than O_2 [35]. The k_{ox} (O_2) of GOX from spinach (8.5×10^4 $M^{-1} \cdot s^{-1}$) [8] is 21-fold lower than the corresponding k_{ox} for wild-type avLOX (Table 2). The Ala95-to-Gly substitution in avLOX therefore creates an oxidase, which in terms of k_{ox} (O_2) is intermediate between wild-type avLOX and GOX. Because reactivity with DCIP compared to O_2 appears to have been strongly enhanced in GOX compared to wild-type avLOX and the same trend in electron acceptor reactivities is observed for the A95G mutant, a structural comparison between GOX and A95G avLOX was suggested.

The crystal structure of spinach GOX is available (PDB code: 1GOX) [3]. A structural comparison of these 36% identical enzymes reveals that the r.m.s.d. between 350 homologous Cα atoms in these monomers is 1.23 Å and so they can therefore be considered to be similar overall. Notably, GOX has an alanine (Ala79) at the equivalent position to the A95G mutation in avLOX and the conformation is similar to the alanine in the wild-type enzyme. Moreover, the flavin ring found in GOX appears to be planar, which has the potential to further restrict binding of larger electron acceptors. Although there is no substrate within the structure of the GOX active site, the residues that potentially interact are in a conformation creating a generally larger active site than the pyruvate-bound A95G active site (Fig. 8B). There are several differences between the active sites that may be able to explain the promiscuous reactivity of GOX. These include the displacement of the Tyr146 (GOX: Tyr129) side chain by 1.8 Å, the Arg181 (Arg164) side chain by 4.6 Å and the His265 (His254) side chain by 1.1 Å away from the pyruvate bound in the avLOX wild-type active site. Another gain of steric volume in GOX results from the lack of residues homologous to Leu211 and Tyr215, which approach the pyruvate within 4.0 and 2.5 Å respectively. It can be concluded from this comparison that there is no common single structural feature or sequence signature that facilitates the binding of larger electron acceptors such as DCIP but rather a general increase in the steric volume of the active site. Therefore, this provides a plausible explanation as to why the A95G variant rather than wild-type avLOX exhibits trend resemblance with GOX in electron acceptor substrate specificities. We also note that, consistent with a scenario where electron acceptor reactivity at the catalytic center is mainly governed by access to the FMN site, the re-oxidation rate constant k_7 did not show an apparent correlation with the intrinsic electronic reactivity (E_m) (Table 2) of the electron acceptor substrate used.

Reactivity with α-hydroxy acid substrates in the reductive half-reaction

Specificity for substituents at position 2 in α-hydroxy acid substrates is assumed to be determined by residues surrounding the methyl group in L-lactate, which includes Ala95 [21,25,43]. Comparison of the A95G avLOX structure with the structure of wild-type enzyme shows that the mutation of this residue to glycine increases the volume available at this position by removing the steric bulk of the alanine side chain and allowing the main chain to relax slightly away from the L-lactate binding site. This extra volume potentially allows the substrate to rotate slightly to permit a re-direction of the substituent at position 2. Moreover,

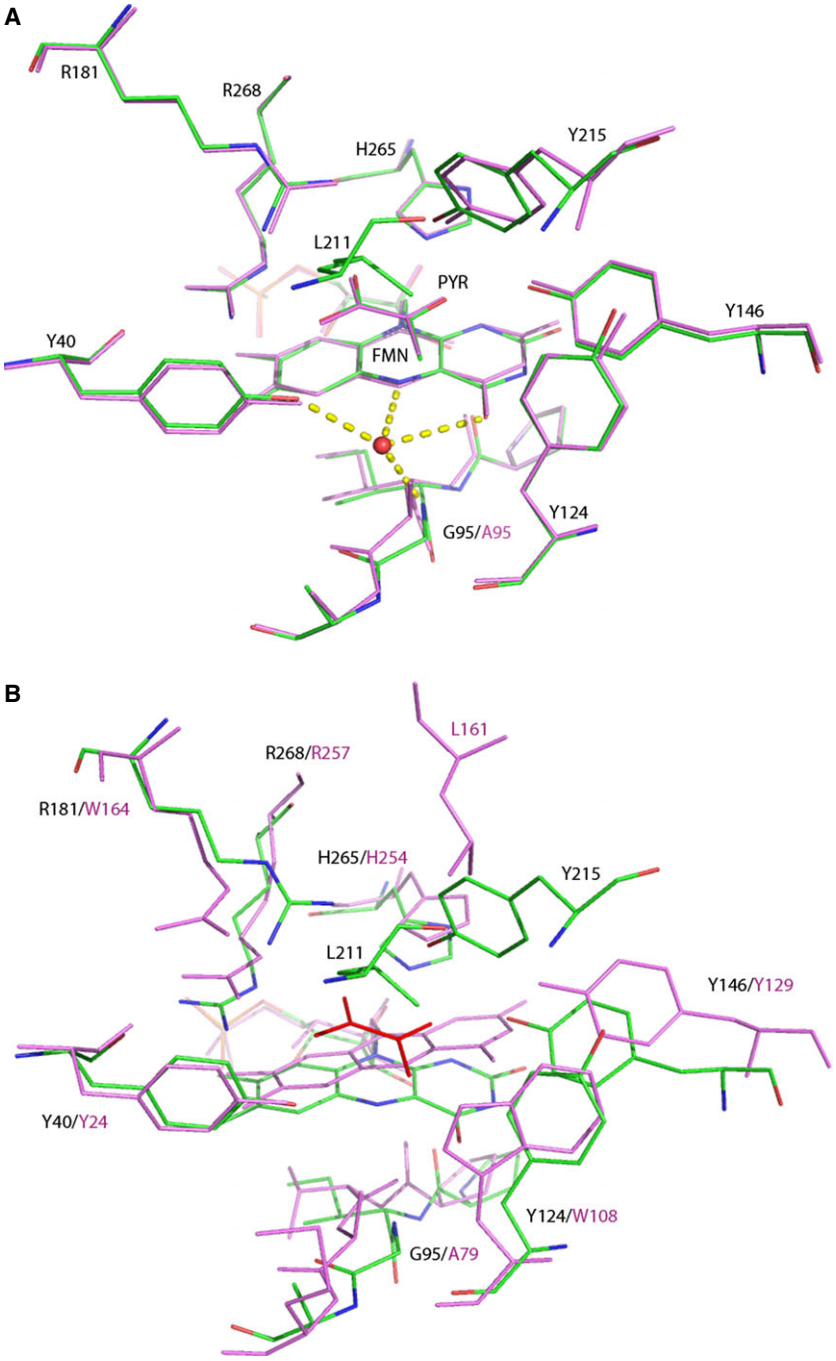

Fig. 8. A comparison of the active sites from wild-type avLOX, the A95G variant and GOX. (A) An overlap of the A subunit (lavender) of the wild-type avLOX structure (PDB code: 2E77) and the A95G variant (colored by atom type) shows the additional steric volume available for DCIP binding as a result of the smaller side chain at position 95, the slightly altered main-chain conformation at that position and the lack of flavin planarity. Leu211 is not present in the wild-type structure as a result of disorder. (B) An overlap of the A95G variant (colored by atom type; pyruvate in red) and GOX (lavender; PDB code: 1GOX) active-site residues surrounding the A95G-bound pyruvate (red) shows the increased steric volume available for electron acceptor binding in GOX versus A95G.

it must be emphasized that the $sp^3 \rightarrow sp^2$ hybridization change at the reactive C2 during substrate oxidation involves substantial reorientation of the C2 substituents when tetrahedral substrate converts via a more planar transition state into planar product. Geometrical requirements of the catalytic reaction coordinate for oxidation of α-hydroxy acid substrates larger than L-lactate are likely to be more easily accommodated by the more spacious binding pocket of A95G avLOX compared to wild-type enzyme. This could explain the mutant enzyme's markedly increased reactivities (k_{red}) with (*S*)-2-hydroxybutyric acid and (*S*)-mandelic acid (Table 1) and generally its higher specificity for larger α-hydroxy acid substrates. It also may account for the decreased efficiency (Table 1) with L-lactate because the substrate would have fewer structural constraints

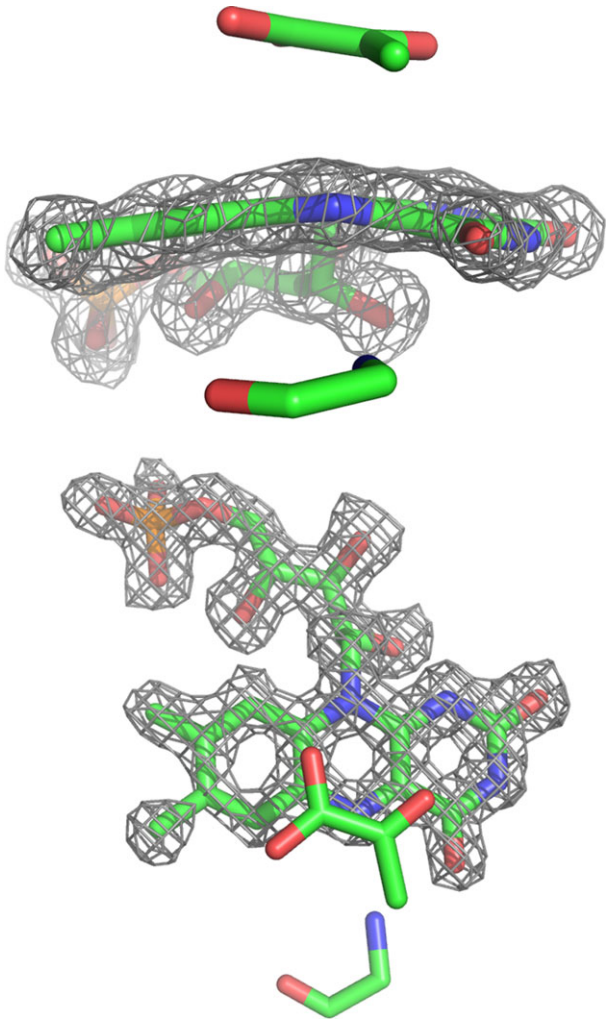

Fig. 9. Unbiased $F_o - F_c$ difference density contoured at 2σ superimposed on the final refined model showing the nonplanarity of the flavin ring. Also shown for reference are the site of the A95G mutation and the bound pyruvate.

in binding and has the potential to bind in a more disordered fashion. Modeling experiments indicate a possible steric conflict between the substituent at position 2 and the side- and/or main-chain atoms of Tyr124 and, to a lesser extent, the side chain of Tyr191. The A95G avLOX crystal structure generally supports the interpretation of kinetic evidence on the A95G variant previously reported by Yorita *et al.* [21,25].

Reactivity with O_2 and alternative electron acceptors in the oxidative half-reaction

The bound FMN and pyruvate molecules are almost completely sequestered from the solvent with calculated accessibilities ranging from 2.2 to 5.2 Å^2 for the FMN and from 0.4 to 3.0 Å^2 for the pyruvate. This implies that there is a conformational change required for the binding and release of pyruvate, as well as for the binding and release of similarly sized electron acceptors. According to the proposed reaction pathway of avLOX (Scheme 1), pyruvate must also dissociate so that O_2 can react with reduced flavin. The region of residues near the range 199–204 is a good candidate for participation in such a conformational rearrangement as a result of its high apparent mobility. Various residues in this segment are often missing in crystal structures and those that are present usually exhibit high temperature factors [3–7,27–29]. In the A95G mutant subunits, certain residues in this region cannot be observed in the electron density: A, 203–204; B, 199–204; C, 203–204; D, 203–204. Although this general region is > 10 Å distant from the pyruvate binding site, it is tempting to speculate that it may function as a hinge region, facilitating the movement of a short helix composed of residues 210–217, which buries the active site from solvent (Fig. 7). This is supported by the high disorder observed in residues 214–217 in subunit C, which prevented the fitting of this segment. Other published structures show similar gaps in this region as well, although some encompass a larger range of 196–213, which includes a portion of the sequestering helix. We also note that, at 4 °C, A95G variant released pyruvate 2.7-fold more slowly than wild-type avLOX did (Table 1).

In flavoenzyme oxidases [18], O_2 is assumed to approach the reactive C4a-N5(H) locus from the edge of the plane in which the FMN molecule lies. In monooxygenases, by contrast, an attack of O_2 is considered to occur from one of the sides (*re* or *si* face) of the cofactor plane and typically involves a well-defined O_2 binding site [18]. Crystal structures of wild-type and A95G lactate oxidases appear to be compatible with both 'edge-on' and 'face-on' approaches of the O_2 substrate to the FMN. However, a *re*-face interaction appears to be unlikely because of steric hindrance from the methyl side chain of Ala95 in wild-type enzyme (Fig. 8A) and bound water in the A95G variant (Figs 1 and 8A), as well as additional protection provided by Pro93 and Ile94. The structures also reveal the absence of a discrete binding pocket for O_2 in the active site, consistent with oxidase-only reaction pathways in both enzymes. To address the decrease in O_2 reactivity in A95G variant compared to wild-type avLOX, it is relevant to consider changes in the local environment of the C4a-N5 locus resulting from the site-directed substitution. The water molecule accomodated in the A95G variant reduces the hydrophobicity around the putative O_2 reacting site compared to the wild-type lactate oxidase that has the methyl group of

Ala95 in an approximately analogous position. For different flavoenzymes, an optimum combination of hydrophobicity and steric constraint creates a physically confined microenvironment that can strongly facilitate the ability of O_2 to rapidly react with the reduced flavin [17,18]. A lowering of polarity of the flavin environment in (*S*)-mandelate dehydrogenase upon substitution of Gly81 by Ala was suggested to account for the slight increase in O_2 reactivity in the mutant compared to wild-type enzyme [44].

The water molecule in A95G avLOX also forms a hydrogen bond with the flavin N5. Studies of other flavin-dependent oxidases/monooxygenases strongly support the idea that hydrogen bonding with the cofactor's N5 atom represents an important strategy for the control of O_2 reactivity [18]. In pyranose oxidase [47], for example, the substitution of a threonine that interacts with the flavin N5 resulted in removal of a characteristic C4a-hydroperoxyflavin stabilization, such that flavin oxidation and H_2O_2 formation occurred without any detectable intermediate, as is normally the case for oxidases. Kinetic isotope effect studies of the pyranose oxidase also suggested that N5-H bond cleavage controls the process of H_2O_2 elimination during flavin oxidation [48]. Hydrogen bonding to N5(H) would consequently disfavor rapid and direct formation of H_2O_2. Thus, installing a hydrogen bond to flavin N5 from water is relatively less effective in altering the reaction with O_2 in avLOX than removing the native hydrogen bond to flavin N5 from threonine in pyranose oxidase, and there is no evidence for C4a-hydroperoxyflavin intermediate formation during O_2 reduction by A95G avLOX. However, hydrogen bonding from water might protect the N5-H proton from proton transfer reactions (e.g. protonation of the departing hydrogen peroxide anion) and this could slow down the overall process of H_2O_2 production from O_2 in A95G variant compared to wild-type avLOX.

With respect to the question of how larger electron acceptors might bind to the active site of the A95G mutant, attempts to manually model DCIP into the binding site were made with particular attention focused on the site of the mutation. Ultimately, it was considered that there were too many possible modes of binding, particularly when possible conformational changes in active site residues were considered. However, there is also the possibility that electron transfer from reduced flavin to DCIP takes place assisted by the protein matrix. In that case, a relatively unspecific interaction between DCIP and the protein might be sufficient for flavin reoxidation to occur. Evidence that DCIP and other alternative electron acceptors reacted with the lactate oxidases in an apparently strictly bimolecular fashion (Fig. 6) supports the notion that specific binding of the acceptor to a discrete binding site in the protein may not have been involved in the electron transfer process from the reduced flavin. The electron transfer between the flavin and the heme group in flavocytochrome b_2 presents a relevant example as it proceeds over a long distance (9.7 Å). It does not involve direct contact between the two chromophores but appears to be aided by protein residues [1,12].

Conclusions

Characteristic Ala/Gly residue variation in the catalytic centers of α-hydroxy acid oxidases has attracted significant attention in structure–function studies of these enzymes, including avLOX. The Ala or Gly adopts a structural position close to the C4a-N5 locus at the *re* face of the FMN cofactor and therefore contributes to the microenvironment of the reaction site. In avLOX, the A95G variant has already been subject of mechanistic investigations. The 1.65-Å crystal structure of A95G avLOX bound with pyruvate provides a detailed interpretation of different kinetic consequences of the site-directed substitution: decreased reactivity with molecular oxygen; increased specificity for reduction of alternative electron acceptors; and increased specificity for oxidation of α-hydroxy acid substrates larger than L-lactate. Generally, from the structural results, it may be concluded that the increased ability of the mutant to utilize larger donor or acceptor substrates is a consequence of the increased steric volume arising from the loss of the alanine methyl group. A comparison of the LOX-A95G structure with the homologous wild-type GOX structure shows that a glycine at this position is not absolutely necessary for the acceptance of alternative electron acceptors such as DCIP as a substrate for this family of enzymes. Lowered O_2 reactivity in A95G variant compared to wild-type avLOX might be a consequence of a hydrogen bond from bound water to flavin N5 in the mutant lactate oxidase, which could protect the N5-H proton in reduced flavin from undergoing proton transfer reactions directly conducive to H_2O_2 elimination in the overall process of O_2 reduction.

Experimental procedures

Materials

The α-hydroxy acids (free acid or sodium salt) and electron acceptors used were of the highest quality available at

Sigma-Aldrich (Deisenhofen, Germany). DCIP was obtained as sodium salt. Solutions of electron acceptors were prepared fresh and kept in the dark prior to use. avLOX wild-type was a kind gift from Roche Diagnostics (Penzberg, Germany). The lyophilized protein was dissolved to a concentration of 10 $mg \cdot mL^{-1}$ in 50 mM potassium phosphate buffer (pH 6.5). The avLOX migrates as a single protein band in SDS/PAGE and was therefore used without further purification. All other materials have been described previously [49].

Construction of A95G avLOX, enzyme production and purification

Plasmid vector pLO-1, which harbors the avLOX gene under control of the tac promoter, was used as template for mutagenesis by a two-stage PCR protocol as reported previously [49]. The two mutagenic oligonucleotide primers used were:

5′-CCAATTGGTGCCCATGGTTTAGCTCACGCTAC TAAAGAAGCTGG-3′ and 5′-AGCGTGAGCTAAACCA TGGGCACCAATTGGGGCCATGATGAATGG-3′.

The mismatched bases are underlined. The desired mutation was verified by sequencing.

Enzyme production was carried out in *E. coli* BL21 (DE3) containing pLO-1 vector encoding wild-type or A95G avLOX. Shaken flask and bioreactor cultivations of the strains, processing of *E. coli* cells and protein purification were carried out by protocols exactly as described previously [49]. Briefly, soluble extract obtained by high-pressure cell disruption was purified by ammonium sulfate precipitation followed by hydrophobic interaction and anion exchange chromatography. Pooled fractions were desalted and concentrated to approximately 20 $mg \cdot mL^{-1}$ in 50 mM potassium phosphate buffer (pH 7.0), using 10-kDa cut-off centrifugal concentrator tubes (Vivaspin 20; Sartorius Vivascience, Göttingen, Germany). Enzymes were stored at −70 °C.

Assays

Protein was measured with Roti-Quant reagent (Carl-Roth, Karlsruhe, Germany) using BSA as reference. The standard LOX activity assay was based on *in situ* peroxidase-coupled detection of the H_2O_2 released during L-lactate (50 mM) oxidation at pH 6.5. It was carried out at 37 °C as described previously [49]. To examine the degree of uncoupling (Scheme 1) in catalytic reactions of wild-type and A95G avLOX, we compared the H_2O_2 formation rate ($r\_H_2O_2$) with the corresponding O_2 consumption rate (r_O_2), considering that, in a fully uncoupled reaction, the absolute value of the rate ratio ($|r\_H_2O_2/r\_O_2|$) is unity. $r\_H_2O_2$ was measured using the coupled peroxidase assay. r_O_2 was measured using a fiber-optic oxygen microoptode (PreSens GmbH, Regensburg, Germany) connected to a miniaturized lock-in amplifier (MICROX TX3), as also obtained from PreSens GmbH. Reactions were performed in magnetically stirred glass vials (total volume of 4.5 mL; 300 r.p.m. agitation rate) sealed air-tight using a septum through which the electrode could be fitted into the system. The total reaction volume was 1.5 mL and air-saturated buffer was used at 37 °C. The L-lactate concentration was 50 mM and fully saturating at steady-state. A 50 mM potassium phosphate buffer (pH 6.5) was used. Reactions were started by injecting a suitably concentrated enzyme solution (10 μL) through the septum and were followed for approximately 3 min. Experimental reaction rates varied between approximately 5.0 and 50 $\mu M \cdot min^{-1}$. The standard error of $r\_H_2O_2$ and r_O_2 determined in identical replicates ($n = 5$) was approximately 5% and 7%, respectively. We found that $r\_H_2O_2$ was equal to r_O_2 within limits of the experimental error.

Because of its comparably lower standard error, $r\_H_2O_2$ was used for determination of Michaelis–Menten parameters. Reaction rates were measured at 10 or more α-hydroxy acid substrate concentrations in the concentration range indicated. Unless noted otherwise, a temperature of 37 °C was used and air-saturated buffer conditions were applied.

Absorbance spectra were recorded with a Varian Cary 50 Bio UV-Vis spectrophotometer (Agilent, Santa Clara, CA, USA) using Hellma quartz cuvettes (Hellma Analytics, Müllheim, Germany) of 10-mm light path. An extinction coefficient of protein bound FMN of 12 500 $M^{-1} \cdot cm^{-1}$ was determined using the protocol reported previously [50]. Enzyme turnover numbers (k_{cat}) are based on the molar concentrations of FMN.

Reaction with DCIP and O_2 as competing electron acceptors

A quartz cuvette closed with a Teflon stopper and fitted with the above-described microoptode was used. The cuvette was placed in the Varian spectrophotometer so that the consumption of DCIP (change in A_{600}) and O_2 (microoptode) could be measured simultaneously over time once the reaction had started via injection of enzyme solution (10 μL). The L-lactate concentration was 50 mM. Air-saturated potassium phosphate buffer ($[O_2] \approx 200$ μM; pH 6.5) was used, and the DCIP concentration was also 200 μM. Reactions were carried out at 37 °C.

Stopped flow experiments

An Applied Photophysics (Leatherhead, Surrey, UK) model SX17MV stopped-flow analyzer equipped with a diode array absorbance detector was used to perform enzyme-monitored turnover experiments. Alternatively,

turnover was determined from absorption measurements at a single wavelength (450 nm, 530 nm) recorded with a photomultiplier detector. Diode array data were recorded every 0.1 ms and the instrument deadtime was below 0.5 ms under the conditions used. Data from diode array measurements (280–700 nm) were deconvoluted using PRO-K software (Applied Photophysics). Anaerobic reaction conditions were established by flushing all solutions exhaustively with nitrogen. Traces of oxygen were removed by adding 10 mM glucose and 200 nM glucose oxidase (Roche Diagnostics). All parts of the stopped-flow apparatus were rinsed with glucose/glucose oxidase solution. A 50 mM potassium phosphate buffer (pH 6.5) was used. Each measurement was repeated five times or more and the stopped-flow traces were averaged.

The reductive half-reaction was followed by collecting spectra with the diode array detector or by measuring the decrease A_{450} after mixing anaerobically the enzyme (final concentration of 5–20 μM) with varied concentrations of α-hydroxy acid substrate [L-lactate, (*S*)-mandelate, (*S*)-2-hydroxybutyrate]. The standard temperature was 20 °C but oxidation of L-lactate was also monitored at 4 °C. The oxidative half-reaction was followed at 20 °C by mixing enzyme, which had been anaerobically reduced by the double molar equivalent of L-lactate, with varied concentrations of electron acceptor substrate (O_2, DCIP, 2,5-dichloro-1,4-benzoquinone, 2,5-dimethyl-1,4-benzoquinone or methyl-1,4-benzoquinone). A_{450} was recorded with the photomultiplier detector, except for reaction with DCIP where diode array data were obtained. Single wavelength traces were fitted to the appropriate single- or double-exponential decay/rise function to obtain pseudo-first-order reaction rate constanst (k_{obs}).

Crystallization, structure determination and refinement

A95G avLOX was crystallized using hanging drop vapor diffusion in air atmosphere at 20 °C. One microliter of protein solution at 10 mg·mL^{-1} in 50 mM potassium phosphate (pH 7.0) was mixed with 1 μL of reservoir solution of 30% polyethylenglycol in 50 mM Tris-HCl buffer (pH 8.0) with the addition of 50 mM pyruvate. Crystals were harvested in 85% (v/v) well solution with 15% (v/v) ethylene glycol. X-ray measurements were carried out at the Stanford Synchrotron Radiation Laboratory (Menlo Park, CA, USA).

Molecular replacement using PHASER [51] was conducted to determine rotation and translation using the avLOX wild-type structure (PDB code: 2DU2) as a search model. Appropriate changes in sequence were made manually to the structure, which was refined using REFMAC5 [52] to reach a final R of 15.4% and R_{free} of 18.0%. Iterations of refinement and manual refitting were used to identify and add waters, ethylene glycol and pyruvate molecules to the structure. PROCHECK analysis was performed as implemented in CCP4I (http://www.ccp4.ac.uk/ccp4i_main.php). WINCOOT 07-PRE 1 [53] was used for fitting and modeling.

Acknowledgements

This work was funded within the Austrian COMET Program under the auspices of the Austrian Federal Ministry of Transport, Innovation and Technology (bmvit); the Austrian Federal Ministry of Economy, Family and Youth (bmwfj); and the State of Styria (Styrian Funding Agency SFG). The COMET Program is managed by the Austrian Research Promotion Agency (FFG). Professor Marco Fraaije (Groningen, The Netherlands) is thanked for introducing T.S. to anaerobic stopped flow methodology. EU COST Action CM0701 'CASCAT' is thanked for providing financial support.

Author contributions

B.N., S.L. and D.K.W. designed the research. T.S. performed the biochemical experiments and analyzed data with S.L. and B.N. Crystallization was performed by D.R. D.R. and D.K.W. determined the structure. B.N. and D.K.W. wrote the paper.

References

1 Palfey BA & Massey V (1998) Flavin-dependent enzymes. In Comprehensive Biological Catalysis: A Mechanistic Reference, Volume III Radical Reactions and Oxidation/Reduction (Sinnott M, ed.), pp. 83–154. Academic Press Limited, London, UK.
2 Lê KHD & Lederer F (1991) Amino acid sequence of long-chain α-hydroxy-acid oxidase from rat kidney, a member of FMN-dependent α-hydroxy-acid-oxidizing enzymes. *J Biol Chem* **266**, 20877–20881.
3 Lindquist Y (1989) Refined structure of spinach glycolate oxidase at 2 Å resolution. *J Mol Biol* **209**, 151–166.
4 Xia Z & Mathews FS (1990) Molecular structure of flavocytochrome b_2 at 2.4 Å resolution. *J Mol Biol* **212**, 837–863.
5 Sukumar N, Dewanti AR, Mitra B & Mathews FS (2004) High resolution structures of an oxidized and reduced flavoprotein. The water switch in a soluble form of (*S*)-mandelate dehydrogenase. *J Biol Chem* **279**, 3749–3757.
6 Umena Y, Yorita K, Matsuoka T, Kita A, Fukui K & Morimoto Y (2006) The crystal structure of L-lactate oxidase from *Aerococcus viridans* at 2.1 Å resolution reveals the mechanism of strict substrate recognition. *Biochem Biophys Res Commun* **350**, 249–256.

7 Cunane LM, Barton JD, Chen Z, Lê KH, Amar D, Lederer F & Mathews FS (2005) Crystal structure analysis of recombinant rat kidney long chain hydroxy acid oxidase. *Biochemistry* **44**, 1521–1531.

8 Macheroux P, Massey V & Thiele DJ (1991) Expression of spinach glycolate oxidase in *Saccharomyces cerevisiae*: purification and characterization. *Biochemistry* **30**, 4612–4619.

9 Maeda-Yorita K, Aki K, Sagai H, Misaki H & Massey V (1995) L-lactate oxidase and L-lactate monooxygenase: mechanistic variations on a common structural theme. *Biochimie* **77**, 631–642.

10 Lockridge O, Massey V & Sullivan PA (1972) Mechanism of action of the flavoenzyme lactate oxidase. *J Biol Chem* **247**, 8097–8106.

11 Lederer F, Belmouden A & Goudry M (1996) The chemical mechanism of flavoprotein-catalysed a-hydroxy acid dehydrogenation: a mutational analysis. *Biochem Soc Trans* **24**, 77–83.

12 Boubacar AKO, Pethe S, Mahy J-P & Lederer F (2007) Flavocytochrome b_2: reactivity of its flavin with molecular oxygen. *Biochemistry* **46**, 13080–13088.

13 Sobrado P & Fitzpatrick PF (2003) Solvent and primary deuterium isotope effects show that lactate CH and OH bond cleavages are concerted in Y254F flavocytochrome b_2, consistent with a hydride transfer mechanism. *Biochemistry* **42**, 15208–15214.

14 Lehoux IE & Mitra B (1999) (*S*)-mandelate dehydrogenase from *Pseudomonas putida*: mechanistic studies with alternate substrates and pH and kinetic isotope effects. *Biochemistry* **38**, 5836–5848.

15 Fitzpatrick PF (2004) Carbanion versus hydride transfer mechanisms in flavoprotein-catalyzed dehydrogenations. *Bioorg Chem* **32**, 125–139.

16 Cao Y, Han S, Yu L, Qian H & Chen J-Z (2014) MD and QM/MM studies on long-chain L-α-hydroxy acid oxidase: substrate binding features and oxidation mechanism. *J Phys Chem B* **118**, 5406–5417.

17 Mattevi A (2006) To be or not to be an oxidase: challenging the oxygen reactivity of flavoenzymes. *Trends Biochem Sci* **31**, 276–283.

18 Chayen P, Fraaije M & Mattevi A (2012) The enigmatic reaction of flavins with oxygen. *Trends Biochem Sci* **37**, 372–380.

19 Sun W, Williams CH Jr & Massey V (1996) Site-directed mutagenesis of glycine 99 to alanine in L-lactate monooxygenase from *Mycobacterium smegmatis*. *J Biol Chem* **271**, 17226–17233.

20 Sun W, Williams CH Jr & Massey V (1997) The role of glycine99 in L-lactate monooxygenase from *Mycobacterium smegmatis*. *J Biol Chem* **272**, 27065–27076.

21 Yorita K, Aki K, Ohkuma-Soyejima T, Kokubo T, Misaki H & Massey V (1996) Conversion of L-lactate oxidase to a long chain alpha-hydroxyacid oxidase by site-directed mutagenesis of alanine 95 to glycine. *J Biol Chem* **271**, 28300–28305.

22 Dewanti AR, Xu Y & Mitra B (2004) Role of glycine 81 in (*S*)-mandelate dehydrogenase from *Pseudomonas putida* in substrate specificity and oxidase activity. *Biochemistry* **43**, 10692–10700.

23 Daff S, Manson FD, Reid GA & Chapman SK (1994) Strategic manipulation of the substrate specificity of *Saccharomyces cerevisiae* flavocytochrome b_2. *Biochem J* **301**, 829–834.

24 Leferink NG, Fraaije MW, Joosten HJ, Schaap PJ, Mattevi A & van Berkel WJ (2009) Identification of a gatekeeper residue that prevents dehydrogenases from acting as oxidases. *J Biol Chem* **284**, 4392–4397.

25 Yorita K, Janko K, Aki K, Ghisla S, Palfey B & Massey V (1997) On the reaction mechanism of L-lactate oxidase: quantitative structure-activity analysis of the reaction with *para*-substituted L-mandelates. *Proc Natl Acad Sci U S A* **94**, 9590–9595.

26 Yorita K, Misaki H, Palfey B & Massey V (2000) On the interpretation of quantitative structure-function relationship data for lactate oxidase. *Proc Natl Acad Sci U S A* **97**, 2480–2485.

27 Li SJ, Umena Y, Yorita K, Matsuoka T, Kita A, Fukui K & Morimoto Y (2007) Crystallographic study on the interaction of L-lactate oxidase with pyruvate at 1.9 Ångstrom resolution. *Biochem Biophys Res Commun* **358**, 1002–1007.

28 Leiros I, Wang E, Rasmussen T, Oksanen E, Repo H, Petersen SB, Heikinheimo P & Hough E (2006) The 2.1 Å structure of *Aerococcus viridans* L-lactate oxidase (LOX). *Acta Crystallogr Sect F Struct Biol Cryst Commun* **62**, 1185–1190.

29 Furuichi M, Suzuki N, Dhakshnamoorhty B, Minagawa H, Yamagishi R, Watanabe Y, Goto Y, Kaneko H, Yoshida Y, Yagi H *et al.* (2008) X-ray structures of *Aerococcus viridans* lactate oxidase and its complex with D-lactate at pH 4.5 show an α-hydroxyacid oxidation mechanism. *J Mol Biol* **378**, 436–446.

30 Minagawa H, Nakayama N, Matsumoto T & Ito N (1998) Development of long life lactate sensor using thermostable mutant lactate oxidase. *Biosens Bioelectron* **13**, 313–318.

31 Romero MR, Ahumada F, Garay F & Baruzzi AM (2010) Amperometric biosensor for direct blood lactate detection. *Anal Chem* **82**, 5568–5572.

32 Hirano K, Yamato H, Kunimoto K & Ohwa M (2001) Design of novel electron transfer mediators based on indophenol derivatives for lactate sensors. *Biosens Bioelectron* **17**, 315–322.

33 Müh U, Massey V & Williams CH Jr (1994) Lactate monooxygenase. I. Expression of the mycobacterial gene in *Escherichia coli* and site-directed mutagenesis of lysine 266. *J Biol Chem* **269**, 7982–7988.

34 Müh U, Williams CH Jr & Massey V (1994) Lactate monooxygenase. III. Additive contributions of active site residues to catalytic efficiency and stabilization of an anionic transition state. *J Biol Chem* **269**, 7994–8000.
35 Schuman M & Massey V (1971) Effect of anions on the catalytic activity of pig liver glycolic acid oxidase. *Biochim Biophys Acta* **227**, 521–537.
36 Rao PS & Hayon E (1973) Experimental determination of the redox potential of the superoxide radical. *Biochem Biophys Res Commun* **51**, 468–473.
37 Dawson RMC, Elliott DC, Elliott WH & Jones KM (1986) Data for Biochemical Research. Oxford University Press, NY.
38 Sollner S, Deller S, Macheroux P & Palfey BA (2009) Mechanism of flavin reduction and oxidation in redox-sensing quinone reductase Lot6p from *Saccharomyces cerevisiae*. *Biochemistry* **48**, 8636–8643.
39 Senda T, Senda M, Kimura S & Ishida T (2009) Redox control of protein conformation in flavoproteins. *Antioxid Redox Signal* **11**, 1741–1766.
40 Røhr AK, Hersleth HP & Andresson KK (2010) Tracking flavin conformations in protein crystal structures with Raman spectroscopy an QM/MM calculations. *Angew Chem Int Ed* **49**, 2324–2327.
41 Gadda G (2012) Oxygen activation in flavoprotein oxidases: the importance of being positive. *Biochemistry* **51**, 2662–2669.
42 Roth JP & Klinman JP (2003) Catalysis of electron transfer during activation of O_2 by the flavoprotein glucose oxidase. *Proc Natl Acad Sci U S A* **100**, 62–67.
43 Mowat CG, Wehenkel A, Green AJ, Walkinshaw MD, Reid GR & Chapman SK (2004) Altered substrate specificity in flavocytochrome b_2: structural insights into the mechanism of L-lactate dehydrogenation. *Biochemistry* **43**, 9519–9526.
44 Sukumar N, Dewanti A, Merli A, Rossi GL, Mitra B & Mathews FS (2009) Structures of G81A mutant form of the active chimera of (*S*)-mandelate dehydrogenase and its complex with two of its substrates. *Acta Crystallogr D Biol Cryst* **65**, 543–552.
45 Dewanti AR & Mitra B (2003) A transient intermediate in the reaction catalyzed by (*S*)-mandelate dehydrogenase from *Pseudomonas putida*. *Biochemistry* **42**, 12893–12901.
46 Urban P, Alliel PM & Lederer F (1983) On the transhydrogenase activity of baker's yeast flavocytochrome b_2. *Eur J Biochem* **134**, 275–281.
47 Pitsawong W, Sucharitakul J, Prongjit M, Tan TC, Spadiut O, Haltrich D, Divne C & Chaiyen P (2010) A conserved active-site threonine is important for both sugar and flavin oxidations of pyranose 2-oxidase. *J Biol Chem* **285**, 9697–9705.
48 Sucharitakul J, Wongnate T & Chaiyen P (2011) Hydrogen peroxide elimination from C4a-hydroperoxyflavin in a flavoprotein oxidase occurs through a single proton transfer from flavin N5 to a peroxide leaving group. *J Biol Chem* **286**, 16900–16909.
49 Unterweger B, Stoisser T, Leitgeb S, Birner-Grünberger R & Nidetzky B (2012) Engineering of *Aerococcus viridans* L-lactate oxidase for site-specific PEGylation: characterization and selective bioorthogonal modification of a S218C mutant. *Bioconj Chem* **23**, 1406–1414.
50 Macheroux P (1999) UV-visible spectroscopy as a tool to study flavoproteins. In Methods in Molecular Biology, vol 131, Flavoprotein Protocols (Chapman SK & Reid GA, eds), pp. 1–7. Humana Press Inc., Totowa, NJ, USA.
51 Collaborative computational project 4 (1994) The CCP4 suite: programs for protein crystallography. *Acta Crystallogr D Biol Cryst* **50**, 760–763.
52 Murshudov GN, Vagin AA & Dodson EJ (1997) Refinement of macromolecular structures by the maximum-likelihood method. *Acta Crystallogr D Biol Cryst* **53**, 240–255.
53 Emsley P, Lohkamp B, Scott WG & Cowtan K (2010) Features and development of COOT. *Acta Crystallogr D Biol Cryst* **66**, 486–501.